IEEE Access
Multidisciplinary | Rapid Review | Open Access Journal

Received August 25, 2018, accepted September 29, 2018, date of publication November 9, 2018, date of current version December 3, 2018.

Digital Object Identifier 10.1109/ACCESS.2018.2877711

Rolling Bearing Fault Diagnosis via ConceFT-Based Time-Frequency Reconfiguration Order Spectrum Analysis

DONGDONG LIU, WEIDONG CHENG, AND WEIGANG WEN
School of Mechanical, Electronic and Control Engineering, Beijing Jiaotong University, Beijing 100044, China

Corresponding author: Weidong Cheng (wdcheng@bjtu.edu.cn)

This work was supported in part by the Fundamental Research Funds for the Central Universities under Grant 2018YJS137 and in part by the National Natural Science Foundation of China under Grant 51275030.

ABSTRACT Bearing vibration signals under nonstationary conditions exhibits time-varying instantaneous frequency (IF) feature, resulting in difficulty in fault characteristic frequency identification. Order tracking (OT) is one of the most prevalent techniques to remove the influence of speed fluctuation. However, it produces different spectrums guided by different IFs, which hinders the fault diagnosis. Generalized demodulation (GD) is another effective method newly proposed to process nonstationary signals. Nevertheless, in the demodulation operation, all phase functions of target frequency components must be required. In fact, it is hard to detect one consistent IF to guide OT, and even harder to estimate all IFs to facilitate GD without tachometer. As such, a novel method is proposed, which can pinpoint all frequency components of interest guided by only one IF, and the result spectrum does not change with the variation of references, i.e., arbitrary IF extracted from the signal can guide the reconfiguration. First, the Hilbert transform is applied to bearing signal to highlight the impulsive components and obtain the envelope signal. Second, the Chirplet path pursuit is adopted to extract one IF from the envelope. Then, the concentration of frequency and time (ConceFT) algorithm is exploited to generate the time–frequency representation (TFR) with sharp time–frequency ridges. Next, the ConceFT-based TFR is reconfigured guided by the extracted IF. Finally, the reconfigured TFR is mapped to the 2-D representation, yielding time–frequency reconfiguration order spectrum. The performance is validated by both simulated and experimental data.

INDEX TERMS Rolling bearing, order spectrum, nonstationary condition, fault diagnosis, time-frequency reconfiguration.

NOMENCLATURE

AM	Amplitude modulation
ConceFT	Concentration of frequency and time
CPP	Chirplet path pursuit
EMD	Empirical mode decomposition
FCC	Fault characteristic coefficient
FCF	Fault characteristic frequency
FM	Frequency modulation
GD	Generalized demodulation
IDMM	Instantaneous dominant meshing multiple
IF	Instantaneous frequency
LSSVM	Least square support vector machine
MMSDE	Multi-scale symbolic dynamic entropy
mRMR	Minimum redundancy maximum relevance
MST	Multitaper synchrosqueezing transform
OT	Order tracking
ST	Synchrosqueezing transform
TF	Time-frequency
TFR	Time-frequency representation
TFRO	Time-frequency reconfiguration order
WT	Wavelet transform

I. INTRODUCTION

Rolling bearings as elemental components of rotating machinery are vulnerable to fault due to the tough running environment, such as high rotating speed, heavy yet unpredictable load, and high temperature [1], [2]. A simple

local fault on the bearing would result in excessive vibration levels or breakdowns of rotating machinery. Therefore, the bearing fault diagnosis has drawn increasing attention owing to its high importance in preventing severe equipment damage and unscheduled downtime.

The condition of the rotating machinery can be detected from acoustic emission [3], thermal [4], oil debris [5], [6], and vibration signal [7], [8]. Among them, the vibration signal is one of the most popular tools to diagnose the rotating machinery. Based on the vibration signal, model-based techniques [9], [10], classification methods [11]–[13] and fault characteristics extraction methods [14], [15] have made significant contribution to the machinery fault diagnosis. Among those methods, fault characteristics extraction methods lie at the foot of all techniques. For example, Li *et al.* [9] employed Wavelet transform (WT) to deal with the coupled fault characteristics of gear pair and applied Autoregressive model to cope with the gear faults. Zhou *et al.* [10] applied shift-invariant dictionary to extract the bearing fault characteristic and then utilized Markov model to recognize the fault type. Li *et al.* [11] utilized multi-scale symbolic dynamic entropy (MMSDE) and minimum redundancy maximum relevance (mRMR) to identify the fault characteristics of planetary gearboxes and then applied least square support vector machine (LSSVM) to complete the fault type classification. These works have contributed a lot to the fault diagnosis. Bearing fault diagnosis under nonstationary conditions is still a challenge in real applications. In this paper, we focus on the fundamental fault characteristic extraction technique of rolling bearing.

Identifying fault characteristic frequency (FCF) is one direct and effective approach to monitoring the bearing [16]. In the Fourier spectrum of raw signal, there are complex sidebands around the resonance frequency according to the modulation feature of bearing vibration and convolution property. Besides the complexity of the spectrum, the random slip further hinders the effectiveness of detecting FCF from the frequency representation of raw signal. Amplitude demodulation can effectively pinpoint the FCF, because it avoids the sidebands and highlights the amplitude of impulsive components. The methods, such as empirical mode decomposition (EMD) based algorithms [17], [18], spectral kurtosis [19], [20], and singular spectrum analysis [21] are developed, which facilitates the envelope analysis. However, the time-varying rotating speed will lead to spectrum smearing, because the energy of FCF or its harmonics is distributed in a certain frequency range, rather than concentrates on a constant frequency value.

Order tracking (OT) is one of the most effective techniques to deal with the spectrum smearing [22]–[27]. The essence of OT lies in resampling the time domain signals equi-angularly guided by the rotating frequency, without considering the magnitude of waveform, i.e., the time-varying trajectories of instantaneous characteristic frequency components are converted into lines parallel to time axis on the time-frequency representation (TFR). Cheng *et al.* [23] utilized OT to resample the product functions obtained by local mean decomposition to extract the gear fault features. Li *et al.* [24] combined OT with sparse decomposition to diagnose the complex planetary gearbox faults under nonstationary conditions. Yang *et al.* [25] employed OT to resample the bearing vibration signals and then applied constrained independent component analysis to deal with the angular domain signal. In the process of interpolation, the rotating frequency as a trigger reference is indispensable. In fact, the reference rotating speed is not always available from the tachometer/encoder, due to the limitations of cost and installation location.

Algorithms used to estimate the instantaneous frequency (IF) from vibration signal are developed to avoid the auxiliary equipment. Due to the fact that the gear meshing frequency is easily observable, they are effectively employed in gearbox diagnosis. Wang *et al.* [28] extracted the gear instantaneous dominant meshing multiple (IDMM) to provide a reference for adaptive noise cancellation algorithm and Zhao *et al.* [29] applied the estimated IDMM to resample the gearbox vibration signals. He *et al.* [30] utilized energy centrobaric correction technique to detect the instantaneous meshing frequency, and then adopted OT to extract gearbox faults. Zhao *et al.* [31] proposed a tacho-less OT technique, in which the Chirplet-based approach is introduced to estimate a harmonic of rotating frequency, to detect the gear fault feature. From bearing signals, it is almost impossible to extract rotating frequency directly. Compared with the rotating speed, FCF can be more easily detected from the envelope. However, according to the principle of OT, it produces different spectra guided by different IFs. Therefore, it is necessary to estimate the rotating speed by the extracted frequency. Nevertheless, the rotating speed is hard to be calculated by the extracted FCF, because the ratio of FCF to rotating speed cannot be determined, if the fault location is uncertain. Moreover, it is hard to claim the detected frequency must be the fundamental frequency, rather than its harmonics [32]. During different periods of operation, the amplitude of its harmonics may be higher. Hence, the ratio of the extracted IF to the rotating speed is not always determined, which results in difficulty in estimating the rotating speed to guide the OT.

Generalized demodulation (GD) is another newly developed algorithm to detect the nonstationary signal [33]. It can convert the time-variant IF into constant one, and then wavelet analysis is applied to the transformed component to improve the time-frequency (TF) resolution. Li and Liang [34] proposed generalized synchrosqueezing transform to avoid the diffusions in the time and frequency dimensions. Feng *et al.* [35] further developed iterative generalized synchrosqueezing transform for improving the TFR resolution of multi-component signal. Inspired by the property of GD, it has been extended to frequency spectrum analysis. Zhao*et al.* [36] utilized GD to reveal the FCF of bearing guided by the measured rotating speed. Feng *et al.* [37] presented an order spectrum analysis based on iterative

generalized demodulation for planetary gearbox fault detection. However, before the application of GD, the phase functions of all target frequency components must be detected. In [36], only mono-component is demodulated referring to the measured rotating speed. Reference [37] estimated the IFs by fitting the observable gear meshing frequency. But it is hard to detect all IFs of bearing vibration signals to calculate the phase functions. Although there are proportional relationships between the FCF and its corresponding rotating frequency, the ratios of the FCFs caused by different parts to the rotating speed are unequal, which hinders the estimation of the other components. Therefore, without the rotating speed serving as a reference, it is difficult to demodulate all the target characteristic frequencies by GD algorithm.

In general, the time-varying feature of bearing signals is always removed in the time domain, no matter by OT or GD. However, this highly relies on the reference IF. OT produces different order spectrums referring to different IFs and it is hard to estimate the rotating frequency by the detected IF. Using GD to detect all target frequency components requires all phase functions, but the phase functions are difficult to determine without the measured speed. In fact, the time-varying behavior is manifested fully in the TFR of the envelope, although the characteristic frequency components with low amplitude magnitude are often overwhelmed by noise. As such, we attempt to remove the time-varying behavior in the TF domain.

In this paper, a simple yet flexible method is proposed to reveal the frequency contents of bearing signal under time-varying rotating speed. It is implemented by the TF reconfiguration with one IF as a trigger reference. To avoid the installation of tachometer/encoder, an ideal IF is extracted from bearing signal by exploiting the merits of the Chirplet path pursuit (CPP) algorithm [38]. Due to the low correlations between chirplet functions and noise, CPP is robust to noise. Moreover, any prior knowledge including the phase and amplitude is not required in the detection operation. Concentration of frequency and time (ConceFT) [39] can provide a fine TFR with sharp TF ridges by locally 'squeezing' the TF distribution. More importantly, it can suppress the spurious TF distribution caused by noise, thus achieving strong robustness to noise. The novelty of the proposed method is that it removes the spectrum smearing in the ConceFT-based TFR domain.

The method is detailed as follows. First, the envelope signal is obtained by applying the Hilbert transform to the signal to highlight the impulsive components. Second, one IF is extracted from the envelope using CPP. Then, the TFR of the envelope with sharp TF ridges is obtained by ConceFT. Next, the ConceFT-based TFR is reconfigured guided by the extracted IF. Finally, the time-frequency reconfiguration order (TFRO) spectrum is obtained by mapping the reconfigured TFR to 2-D representation. Based on the TFRO spectrum, the fault pattern is identified.

Hereafter, this paper is organized as follows. In Section II, the background knowledge is introduced. In Section III, the ConceFT-based TFRO spectrum in bearing fault detection is proposed. In Section IV, the method is illustrated via simulated signals. In Section V, the method is further validated by experimental signal. The conclusions are drawn in Section VI.

II. BACKGROUND KNOWLEDGE

A. THE MODULATION CHARACTERISTICS OF BEARING SIGNALS

To pinpoint the fault feature, it is necessary to revisit the modulation characteristics of the bearing vibration signal. In general, if a local fault occurs to a rolling bearing, a series of impulses is generated by the collision between the defective point and its matching ball. The repetition frequency of impulses is called FCF [40]. Under a certain rotating speed, the value of FCF is only determined by fault location and geometric parameters of the bearing.

Rolling bearing signals exhibit amplitude modulation (AM) and frequency modulation (FM) features. The frequency spectra of raw signals consist of intricate sidebands around the resonance frequency because of the modulations and the convolution property, thus making it difficult to detect FCF from the sideband spacing. Amplitude demodulation highlights the impulsive component. However, the obtained spectrum will be blurred under time-varying speed. Under constant rotating speed, as is shown in Fig. 1 (a), clear TF ridges of characteristic frequency components, whose trajectories are parallel to time axis, appear on the envelope TFR plane. Correspondingly, prominent peaks are revealed in the envelope spectrum. When the speed fluctuates, as is

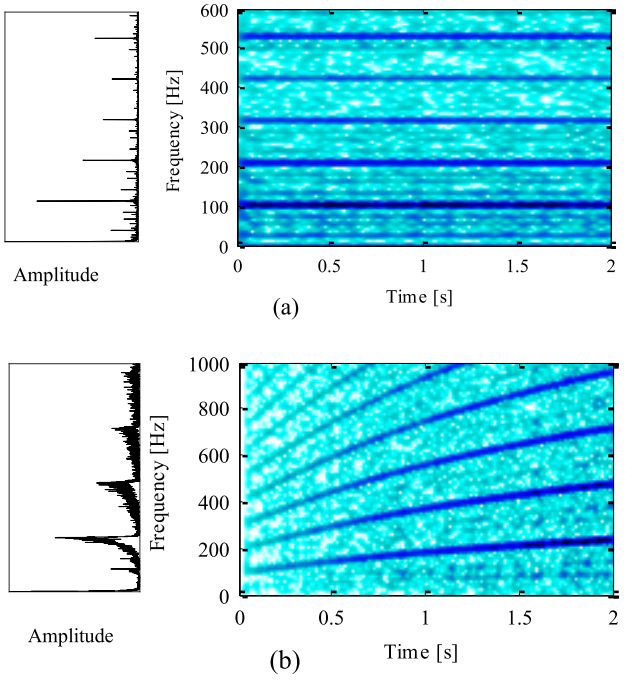

FIGURE 1. (a) Envelope TFR under constant rotating speed, (b) envelope TFR under time-varying rotating speed.

shown in Fig. 1 (b), the IF trends change following the speed variation profile (i.e., the energy of characteristic frequency is distributed in a certain frequency range, rather than concentrating on a constant frequency value). Therefore, no obvious peak is revealed in the envelope frequency representation.

B. THE SIGNAL PROCESSING METHODS FOR TIME-VARYING BEARING SIGNALS

In this section, the commonly used methods, OT and GD, especially their principles and drawbacks for processing time-varying bearing signals, are introduced.

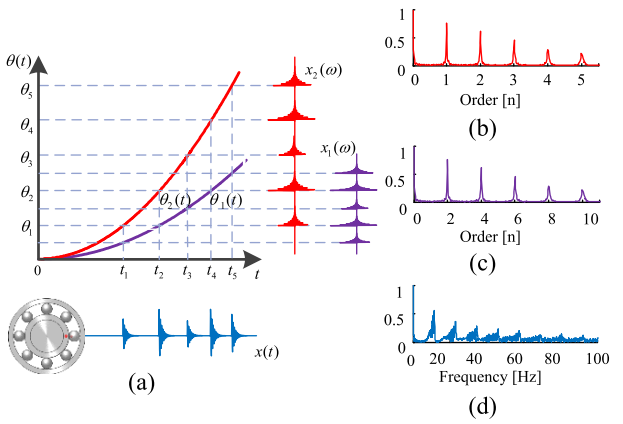

FIGURE 2. Observations of OT illustrated with an example: (a) the principle of resampling, including the raw impulse series $x(t)$ (in blue), the integral curves $\theta_1(t)$ (in purple) and $\theta_2(t)$ (in red), the impulse series $x_1(\omega)$ and $x_2(\omega)$ in angular domain guided respectively by f_r and f_{fcf}, (b) and (c) are the order spectra of $x_2(\omega)$ and $x_1(\omega)$ respectively, (d) the envelope spectrum of $x(t)$.

OT converts time-varying frequency components of bearing vibration signals to constant ones guided by the synchronous rotating frequency. For a bearing signal $x(t)$ (shown in Fig. 2 (a)) under increasing rotating frequency $f_r(t)$, the envelope spectrum of $x(t)$is plotted in Fig. 2 (d). In this figure, no prominent peak is revealed. Guided by the rotating speed, the resampled signal $x_1(\omega)$ is obtained by interpolating $x(t)$ based on the rotated angle $\theta_1(t) = 2\pi \int f_r(t)\mathrm{d}(t)$. From the order spectrum of $x_1(\omega)$, illustrated in Fig. 2 (c), it can be observed that some prominent peaks are revealed at the order value 2 and its multiples. This indicates OT can remove the spectrum smearing effect caused by speed fluctuation, and then identify the fault pattern.

According to the definition of OT, $O = f/f_r$(O is the order, f is the frequency of time domain signal, f_r is rotating speed), arbitrary IF proportional to the rotating speed can be applied to guide the resampling. The angular domain signal $x_2(\omega)$ is obtained by resampling $x(t)$ guided by FCF (the integral function $\theta_2(t) = 2\pi \int f_{\mathrm{fcf}}(t)d(t)$ is plotted in Fig. 2 (a)). In the corresponding order spectrum (Fig. 2 (b)), though some peaks are revealed, the values of those orders have changed. Therefore, guided by different IFs, the obtained order spectra are different. To accurately localize the fault, it is necessary to estimate the rotating speed, if the rotating speed cannot be measured. However, as mentioned before, it is hard to calculate the rotating speed by the IF, due to the uncertain ratio of the IF to the corresponding rotating frequency.

GD is another effective method that can map the time-varying IF to constant component. To illustrate this method, a simple multi-component signal $x(t)$ is generated.

$$x(t) = \sum_{i=1}^{N} A_i \sin[2\pi \int f_i(t)t\mathrm{d}(t)] \quad (1)$$

$$f(t) = -4.5t^6 + 46t^4 - 189t^2 + 167.2t + 18.2 \quad (2)$$

where A_i represents the amplitude, $f_i(t)$ is the IF of the signal, $N = 3$. The signal $x(t)$ can be regarded as a signal composed by the IF $f_1(t) = f(t)$, its second harmonic $f_2(t)$ and third harmonic $f_3(t)$.

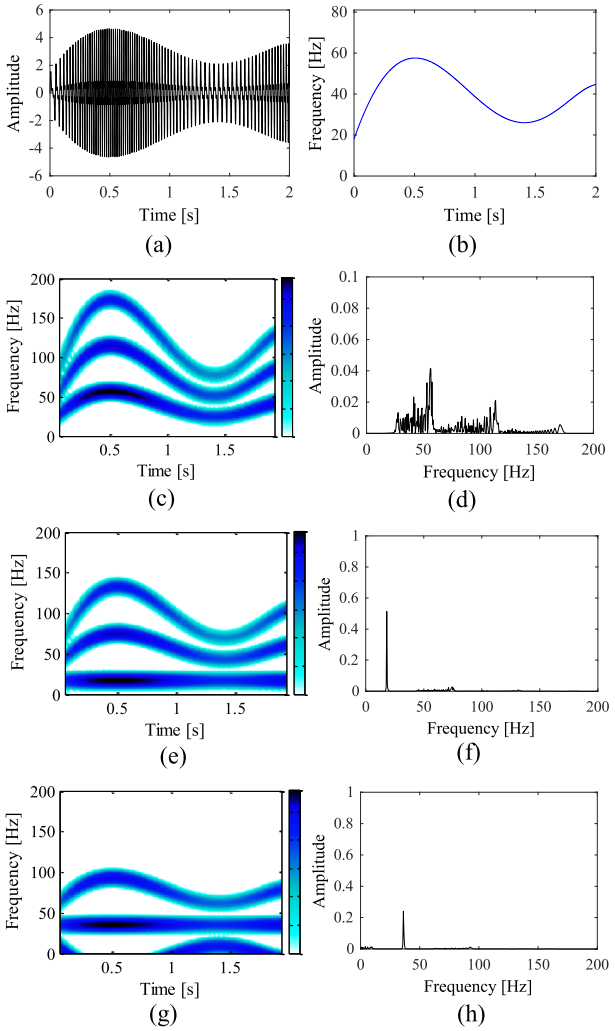

FIGURE 3. The illustration of GD: (a) waveform of signal $x(t)$, (b) IF $f_{1(t)}$, (c) TFR of $x(t)$, (d) frequency spectrum of $x(t)$, (e) and (g) are the TFRs of demodulated signals guided by $v_1(t)$ and $v_2(t)$ respectively, (f) and (h) are the frequency spectra of demodulated signals guided by $v_1(t)$ and $v_2(t)$ respectively.

Fig. 3 (a) and (b) show the waveform of $x(t)$ and the fundamental frequency $f(t)$respectively. The short time Fourier transform (STFT) based TFR and the frequency

spectrum of $x(t)$ are plotted in Fig. 3 (c) and (d) respectively. It can be observed that there is no obvious peak in the frequency spectrum. The demodulated signal $y_1(t) = x(t)\exp[-\mathrm{j}2\pi v_1(t)]$ is constructed based on the phase function $v_1(t) = \int [f_1(t) - f_0]\mathrm{d}(t)$. Fig. 3 (e) shows the TFR of $y_1(t)$. The trajectory of $f_1(t)$ is mapped into a line parallel to the time axis. Correspondingly, as Fig. 3 (f) shows, $f_1(t)$ is revealed in frequency spectrum. Similarly, $f_2(t)$ can be mapped to a constant frequency guided by $v_2(t) = \int [f_2(t) - f_0]\mathrm{d}(t)$. The TFR and the frequency spectrum of the corresponding demodulated signal are shown in Fig. 3 (g) and (h). Therefore, based on a given phase function, only one time-varying frequency component can be demodulated to a constant frequency.

However, it is difficult to detect all frequency components. As mentioned before, there are proportional relationships among the FCF, rotating frequency as well as their harmonics. However, the ratios of the FCFs caused by different parts to the rotating speed are unequal, which hinders the estimation of the other components. In addition, it is hard to claim that the detected frequency is the fundamental frequency, not its harmonics. Therefore, the application of GD is essentially subject to the phase function estimation.

III. CONCEFT-BASED TFRO SPECTRUM

Both OT and GD remove the smearing effect by mapping the time-varying frequency components to instant ones guided by a certain IF. Inspired by this idea, a simple yet flexible ConceFT-based TFRO approach is proposed in this section. Compared to OT and GD, the method can reveal the frequency contents guided by only one arbitrary IF detected from the nonstationary signal.

A. EXTRACTION OF IF USING CPP

For a nonstationary vibration signal of bearing, in theory, the time-varying behavior is reflected in one arbitrary IF. Therefore, we exploit the robustness of the CPP to noise to detect one successive IF from the envelope. Given a bearing signal $x(t)$, the amplitude of the characteristic frequency is highlighted by the envelope demodulation. Then, the CPP is used to detect one IF by joining a series of chirplet atoms in a dictionary defined by

$$f_{a,b,I}(t) = |I|^{-1/2}\exp[-\mathrm{i}(a_\mu t^2/2 + b_\mu t)]L_I(t) \tag{3}$$

where I is the dynamic interval, $I = [kT2^{-j}, (k+1)T2^{-j}]$, j is the scale factor, $j = 0, 1, \cdots, \log_2 N - 1$, T is the total time, $k = 0, 1, \cdots, 2^{j-1}$, a_μ and b_μ are the slope and offset parameters respectively. $L_I(t)$ is a rectangular window function, if $t \in I$, $L_I(t) = 1$, if $t \notin I$, $L_I(t) = 0$. $I^{-1/2}$ is normalization factor, resulting in $\|f_{a,b,I}(t)\|_{L_2} = 1$ ($\|\cdot\|$ is the Euclidean norm).

According to (3), the IF of chirplet atom can be calculated $a_\mu t + b_\mu$. The CPP is implemented by finding a best way to linking the atoms together piece by piece to appropriate the IF of a signal. The selecting chirplet atoms group should be most relevant to $y(t)$. It is satisfied by the maximum coefficient

$$\beta_I = \max_I \langle y(t), f_{a,b,I}(t)\rangle \tag{4}$$

where $\langle\cdot\rangle$ represents the inner product. Then the component represented by β_I can be calculated

$$d(t) = |\beta_I|\exp[-\mathrm{i}(at^2 + bt) + \angle\beta_I]L_I(t) \tag{5}$$

If $\Pi = \{P_1, P_2, \cdots, P_M\}$ is a set of all possible paths to approach $y(t)$, the joining path $P_m\big|_{m=1,2,\cdots,M}$ covering the time span L satisfies

$$d(t) = \arg\max_{m=1,2,\cdots,M} \|d_m(t)\|^2 \tag{6}$$

where $\|\cdot\|$ represents the Euclidean norm, the connecting path of $d_m(t)$ is P_m. The IF of the signal can be estimated by joining the liner frequencies of chirplet atoms in the path in order.

B. TFR USING CONCEFT

To achieve an order spectrum of high quality, a fine TFR is necessary. To date, various TF analysis methods have been developed. However, the conventional methods suffer from their inherent limitations [41]. For example, linear TFRs [42], [43], such as STFT and WT, are limited to Heisenberg uncertainty principle and cannot achieve high resolution in time and frequency scales simultaneously. Bilinear TFRs [44], [45], such as Cohen and Wigner-Ville distribution, are subject to interference terms among frequency components in the TF domain.

To improve the TF resolution, Daubechies *et al.* [46] proposed synchrosqueezing transform (ST). It produces a better TF resolution by squeezing the TFR in a proper scale range, thus removing the blur in the scale/frequency domain. However, the performance of synchrosqueezing degrades when the signals with strong noise are processed, because the noise obscures the concentration of true frequency components. To strengthen the robustness to noise, recently, Daubechies *et al.* [39] further proposed ConceFT, which can effectively suppress the spurious distribution of noise and then achieve a high quality TFR. Therefore, we conduct ConceFT to obtain a TFR with sharp TF ridges of bearing signal.

The WT of the signal $y(t)$ can be given by

$$W_y(a,b) = \langle y(t), \psi_{a,b}(t)\rangle = \frac{1}{\sqrt{a}}\int_{-\infty}^{+\infty} y(t)\psi^*(\frac{t-b}{a})\mathrm{d}t \tag{7}$$

where a is the scale, b is the time offset, $\psi(t)$ is the selected wavelet, $*$ denotes complex conjugate operation. If $y(t) = \cos(\omega t)$, (7) can be recast as

$$\begin{aligned} W_y &= \frac{\sqrt{a}}{2\pi}\int_{-\infty}^{+\infty} \widehat{y}(\xi)\widehat{\psi}^*(a\xi)\exp(ib\xi)d(\xi) \\ &= \frac{A\sqrt{a}}{4\pi}\widehat{\psi}^*(a\omega)\exp(ib\omega) \end{aligned} \tag{8}$$

If the energy of $\widehat{\psi}(\xi)$ is concentrated around the frequency $\xi = \omega_0$, $W_y(a,b)$ will be concentrated around $a = \omega_0/\omega$

on the time-scale plane. However, the $W_y(a, b)$ will be distributed around the horizontal line $a = \omega_0/\omega$. Although $W_y(a, b)$ is distributed around a, the oscillatory behavior of $W_y(a, b)$ in b points to the original frequency ω, not subject to the value of a.

Therefore, the IF $\omega(a, b)$ at any location (a, b) for which $W_y(a, b) \neq 0$ can be computed by

$$\omega(a, b) = \frac{-\mathrm{j}}{W_y(a, b)} \frac{\partial W_y(a, b)}{\partial b} \tag{9}$$

To condense the blur along the scale, according to $\omega(a, b) \to (b, \omega_y(a, b))$, the time-scale plane is transferred to the TF plane. The ST is performed to reassign the time-scale plane to TF plane

$$ST_y(\omega_l, b) = \frac{1}{\Delta\omega} \sum_{a_k} W_y(a_k, b) a_k^{-3/2} (\Delta a)_k \tag{10}$$

where a_k is the kth discrete scale value, with $(\Delta a)_k = a_k - a_{k-1}$, ω_l is the lth center frequency, $\Delta\omega = \omega_l - \omega_{l-1}$.

In the ST based TFR, the dominant component usually has the similar TF structure. However, the noise varies from reference wavelet to reference wavelet, because WT is a convolution with a wavelet. Inspired by the property, multitaper synchrosqueezing transform (MST) is developed.

$$MST(\omega, b) = \frac{1}{I} \sum_{i=1}^{I} ST^{(\psi_i)}(\omega, b) \tag{11}$$

where I represents the number of reference wavelets $\psi(t)$. The TF distribution artifacts caused by noise are restrained by averaging over a large number of reference wavelets. However, the smeared area on the TF plane will also increase the number of wavelets.

To overcome the limitations of MST, ConceFT method is proposed. For $\psi(t) = \sum_{i=1}^{I} r_i \psi_i(t)$, the synchrosqueezing operation can be used (where the weight r_i is real), but the synchrosqueezing is a highly nonlinear operation. For different choices of vector $\mathbf{r} = (r_1, \cdots, r_I)$, the TFR artifacts due to noise interference. Therefore, the noise artifacts can be limited by averaging over many choices of $\mathbf{r}$. Then the ConceFT algorithm is detailed as follows:

1) Select I orthonormal wavelets $\psi_i(t)$ $(i = 1, \cdots, I)$ with good concentration on the TF plane.
2) Pick N random vectors of unit norm $\mathbf{r}_n$, $n = 1, \cdots, N$.
3) For $n = 1, \cdots, N$, define $\psi_n(t) = \sum_{i=1}^{I} r_{ni} \psi_i(t)$ and calculate the corresponding WT $W_y^{(\psi_n)}(a, b) = \sum_{i=1}^{I} r_{ni} W_y^{(\psi_i)}(a, b)$.
4) Calculate the IF $\omega^{(\psi_n)}(a, b)$ and the corresponding ST $ST_y^{(\psi_n)}(\omega_l, b)$.
5) Average over the random vectors $\mathbf{r}_n$ and then obtain the ConceFT representation

$$CFT_y(\omega, t) = \frac{1}{N} \sum_{n=1}^{N} ST^{(\psi_n)}(\omega, t) \tag{12}$$

In real application, the number of reference wavelets I could be as small as 2, while the number of weight vectors N could be chosen as large as the user wishes to average out the noise artifacts. This method not only effectively sharpens the TF ridges on the TFR of ConceFT, but also suppresses the spurious distribution caused by noise in the synchrosqueezing operation.

C. CONCEFT-BASED TFRO SPECTRUM

In this section, a simple yet flexible method is proposed to reveal the frequency contents of bearing signals under time-varying rotating speed. It is implemented by the TF reconfiguration in the ConceFT-based TFR with one IF as a trigger reference. Given the frequency range is $[\omega_a, \omega_b]$, $f(t)$ is one arbitrary IF detected from $y(t)$ via CPP. The times of the minimum frequency $f_{\min}$ and maximum frequency $f_{\max}$ values of $f(t)$ can be calculated

$$\begin{cases} t_{\min} = \arg\min[f(t)] \\ t_{\max} = \arg\max[f(t)] \end{cases} \tag{13}$$

where $t_{\min}$ and $t_{\max}$ represent the time points of $f_{\min}$ and $f_{\max}$ respectively.

Given the frequency region of interest is $[\omega_a, \omega_b]$, the frequency range of reconfiguration should be smaller than this region, otherwise, the reconfiguration range will exceed the interest frequency region. The scale coefficients of the potential reconfigured minimum and the maximum IFs to the detected IF α and β can be derived from

$$\begin{cases} \alpha = \omega_a / f(t_{\min}) \\ \beta = \omega_b / f(t_{\max}) \end{cases} \tag{14}$$

The frequency region of reconfiguration can be calculated $[\alpha f(t), \beta f(t)]$. After the reconfiguring operation is conducted, all time-varying IFs are converted to constant ones parallel to the time axis. Therefore, the time-varying frequency range on the TFR plane is calculated $[\alpha f(0), \beta f(0)]$. Then the amplitude of the reconfigured TFR $A_{\mathrm{re}}(t, \omega)$ is derived guided by $f(t)$.

$$A_{\mathrm{re}}(t, \omega) = A(t, \omega \frac{f(t)}{f(0)}) \; (\alpha f(0) \leq \omega \leq \beta f(0)) \tag{15}$$

where $A(t, \omega)$ represents the ConceFT-based TFR of signal $y(t)$. Finally, the amplitude of the reconfigured TFR is mapped to 2-D picture

$$Y_{\mathrm{re}}(\omega_i) = \sum_{i=0}^{N} \frac{A_{\mathrm{re}}(t_i, \omega_i)}{N} \tag{16}$$

where $Y_{\mathrm{re}}(\omega_i)$is the TFRO representation, t_i is the time at ith sampling point, ω_i is the frequency at t_i, N is the total sampling points.

The flowchart of the method in bearing fault diagnosis is shown in Fig. 4, which can also be summarized as follows:

1) Apply Hilbert transform to the vibration signal $x(t)$ for highlighting the impulsive components to obtain the envelope signal $y(t)$.
2) Extract one IF $f(t)$ from the signal $y(t)$ using CPP.

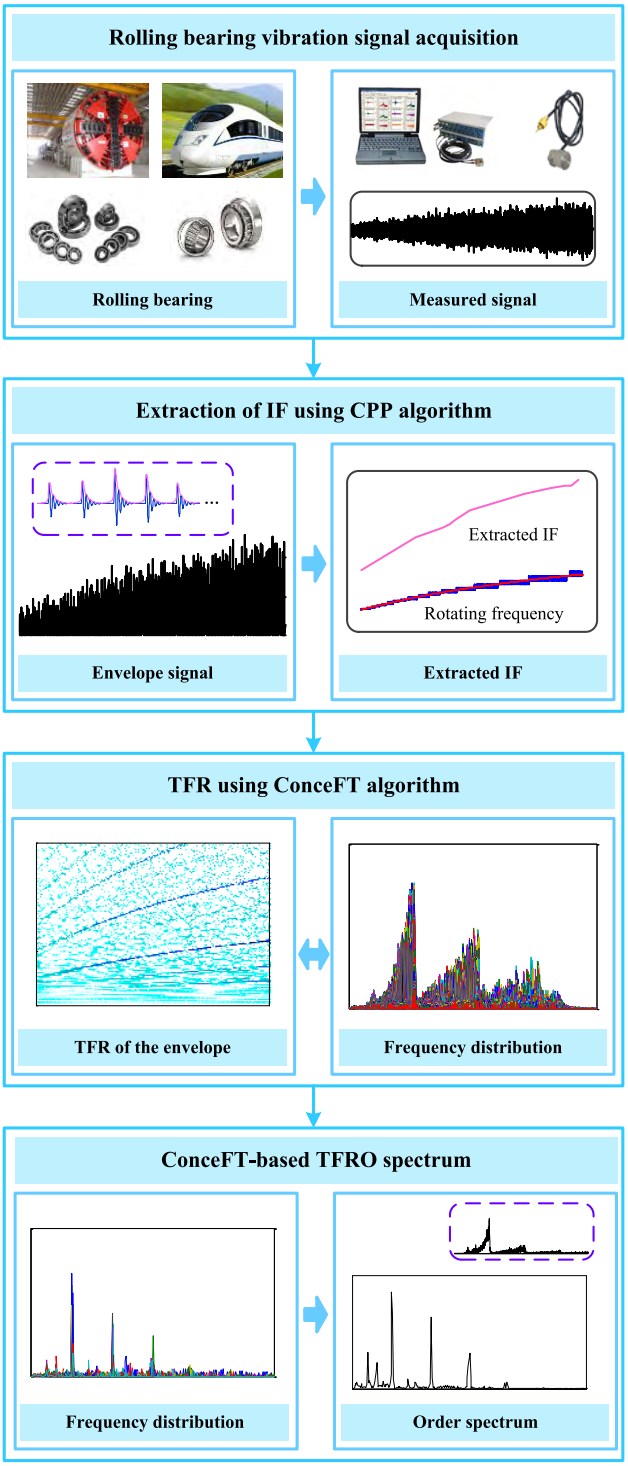

FIGURE 4. Flowchart of the proposed method.

3) Perform ConceFT to the frequency range $[\omega_a, \omega_b]$ of signal $y(t)$ to obtain the TFR $CFT_y(\omega, t)$.
4) Apply the TF reconfiguration to the amplitude $A_y(\omega, t)$ in frequency range $[\omega_a f(0)/f(t_{\min}), \omega_b f(0)/f(t_{\max})]$ obtaining the reconfigured amplitude $A_{\text{re}}(\omega, t)$.
5) Map the amplitude function $A_{\text{re}}(\omega, t)$ to 2-D picture $Y_{\text{re}}(\omega)$ obtaining the TFRO spectrum of $y(t)$.

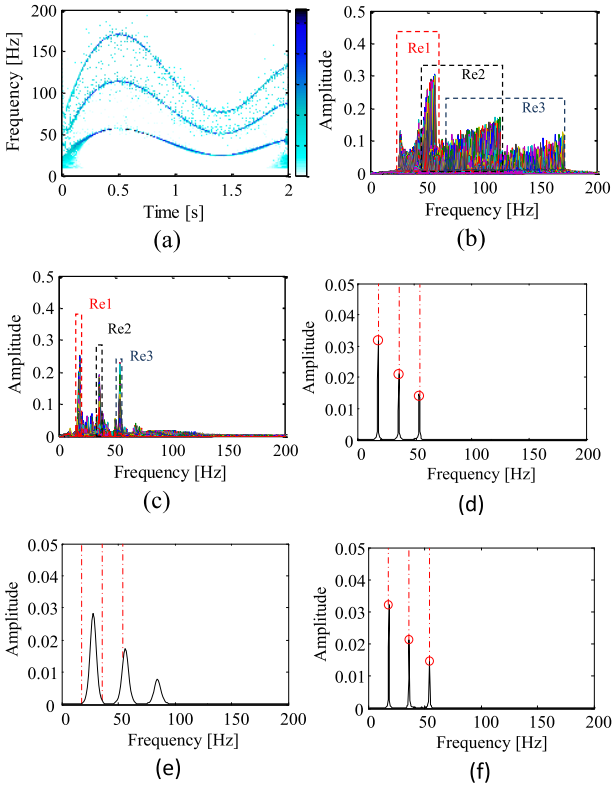

FIGURE 5. Demonstration of ConceFT-based TFRO algorithm: (a) ConceFT-based TFR, (b) frequency spectrum by projecting the TFR, (c) frequency spectrum by projecting the reconfigured TFR, (d) ConceFT-based TFRO spectrum guided by $f_1(t)$, (e) STFT-based TFRO spectrum, (f) ConceFT-based TFRO spectrum guided by $f_2(t)$.

6) Identify the bearing fault pattern by the TFRO spectrum.

To illustrate the method figuratively, the signal generated by (1) is further processed. Fig. 5 (a) shows the ConceFT-based TFR. Compared with Fig. 3 (c), the STFT-based TFR, the TF ridges are sharper. Fig. 5 (b) shows the projection of the TFR onto frequency axis. From this figure, the energy of $f_1(t), f_2(t)$, and $f_3(t)$ is distributed in region (Re) 1, Re 2, and Re 3, rather than in narrow bands, which is the immediate cause of spectrum smearing. The projection of the reconfigured TFR is plotted in Fig. 5 (c). Compared with Fig. 5 (b), the frequency bands are condensed. However, the direct projection operation is sensitive to the background noise. Fig. 5 (d) shows ConceFT-based TFRO spectrum guided by $f_1(t)$, in which the frequency components are pinpointed as expected. However, in the STFT-based TFRO spectrum (Fig. 5 (e)), the result is unsatisfying due to the limitation of Heisenberg uncertainty principle. Fig. 5 (f) shows the TFRO spectrum guided by $f_2(t)$, which is almost identical to the spectrum guided by $f_1(t)$

Based on the analysis above, the advantages of the proposed method are concluded as follows: (a) It avoids the spectrum smearing caused by the IF fluctuation and produces a quality spectrum with prominent yet condensed peaks, which

can be confirmed by Fig. 3 (d) and Fig. 5 (f); (b) It, better than OT, generates a consistent spectrum guided by different IFs, which can be concluded by comparing the OT-based spectra (Fig. 2 (b) and (c)) with the TFRO spectra (Fig. 5 (d) and (f)); (c) Outperforming GD, it pinpoints all time-varying frequency components guided by only one IF, which can be observed from the GD-based spectra (Fig. 3 (f) and (h)) and TFRO spectra (Fig. 5 (d) and (f)).

IV. SIMULATION EVALUATION

In this section, to evaluate the effectiveness of the proposed ConceFT-based TFRO method in analyzing bearing vibration signals, the numerical simulated bearing signals under time-varying rotating speed are generated according to the model

$$x(t) = (1 + \cos(2\pi f_{\mathrm{r}}(t))) \cdot \sum_{\mathrm{m}=1}^{N} A_m \exp(-\beta(t - t_m)) \times \sin(w_{\mathrm{r}}(t - t_m))u(t - t_m) + n(t) \quad (17)$$

where $f_{\mathrm{r}}(t)$ denotes the rotational speed of the bearing, $f_{\mathrm{r}}(t) = -29(t-0.6)^2+29$, A_m the amplitude of the mth impulse, N the number of impulses, $u(t)$ a unit step function, β the damping characteristic, w_{r} the bearing high resonance frequency, $n(t)$ the white Gaussian noise, t_{m} time of mth impulse, which can be calculated by

$$\begin{cases} t_1 = (1+\tau) \cdot 1/(f_{\mathrm{r}}(t_0))/n \\ t_m = (1+\tau) \cdot 1/(f_{\mathrm{r}}(t_{m1}))/n \quad m = 2, 3, \cdots, N \end{cases} \quad (18)$$

where τ is the random slippage effect caused by rolling elements, n is the number of impulses per shaft rotation. Assuming one fault occurs to the outer race, $n = 3.5$, that means the outer race FCF $f_{\mathrm{outer}}(t) = 3.5f_{\mathrm{r}}(t)$. The potential inner race FCF $f_{\mathrm{inner}}(t) = 5f_{\mathrm{r}}(t)$. The detailed parameters are listed in Table 1.

TABLE 1. Detailed parameters of the simulation model.

Sampling frequency	Resonance frequency	Damping coefficient	FCF of outer race	Error coefficient
10 000 Hz	2 000 Hz	900	$3.5\times f_{\mathrm{r}}$	0.01

To better illustrate the principle of the method, a Gauss noise is added to the model with the signal-to-noise ratio (SNR) of 10 dB. Fig. 6 (a) and (b) show the waveform and the TFR of the simulated signal. As the TFR depicts, the energy of the signal is mainly concentrated on the vicinity of resonance frequency 2 000 Hz. However, no TF ridge related to the bearing fault is revealed. Fig. 6 (c) shows the TFR of the envelope by applying Hilbert transform and ConceFT to the signal. In the TFR, clear characteristic frequency ridges are unveiled. Nevertheless, it is hard to identify and localize the fault symptom only based on the TF ridges, especially when the noise level is high. In engineering applications, the rotor unbalance even the manufacturing errors may generate the IF trends in the TFR of the envelope.

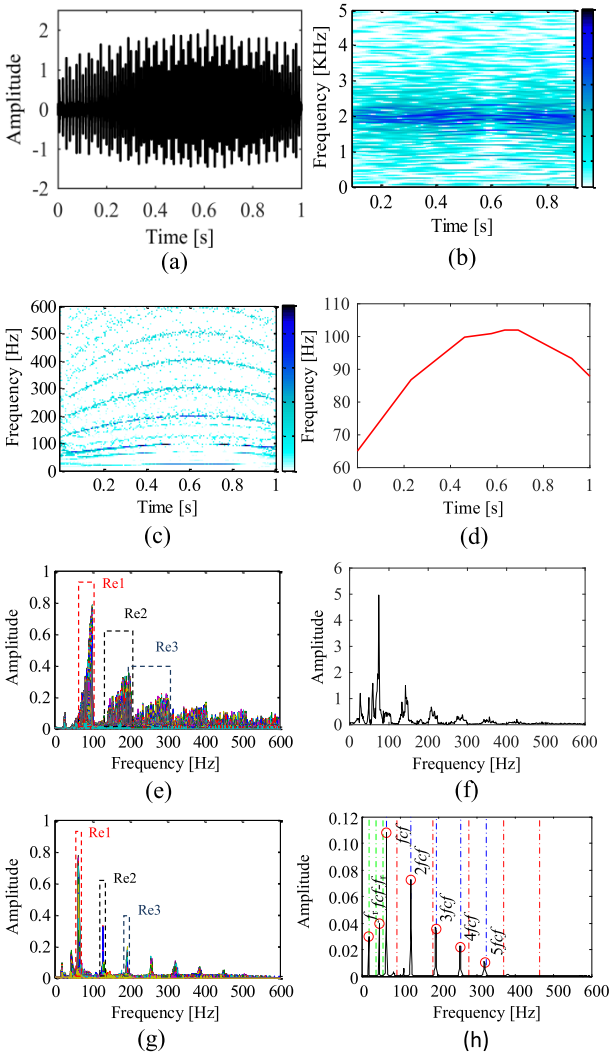

FIGURE 6. Simulated case under SNR = 10 dB: (a) waveform of the simulated signal, (b) TFR of the raw signal, (c) TFR of the envelope signal, (d) IF extracted by CPP, (e) and (f) are the spectra without the TF reconfiguration, (g) and (h) are the spectra based on TFRO method.

The transform results of the TFR to frequency representation without the TF reconfiguration operation are displayed in Fig. 6 (e) and (f). In those spectra, no prominent peak is revealed. Applying CPP to the envelope signal in time domain yields one IF trend plotted in Fig. 6 (d). The trajectory of the extracted IF is consistent with the frequency variation profile in the TFR of the envelope. Regardless of the cause of the detected frequency trend (FCF, its harmonic or the rotating speed), TFRO method is applied directly to the envelope TFR guided by the detected IF so as to yield the projection spectrum and the order spectrum, plotted in Fig. 6 (g) and (h) respectively. In the TFRO order spectrum, prominent peaks appear at the location of f_{r}, $nfcf$, and $fcf - f_{\mathrm{r}}$ as expected. The fault location can be determined by the ratio of fcf to $f_{\mathrm{r}}(C_{\mathrm{outer}} = fcf/f_{\mathrm{r}})$. This confirms that the method can remove the spectrum smearing and pinpoint all frequency components guided by only one extracted IF trend.

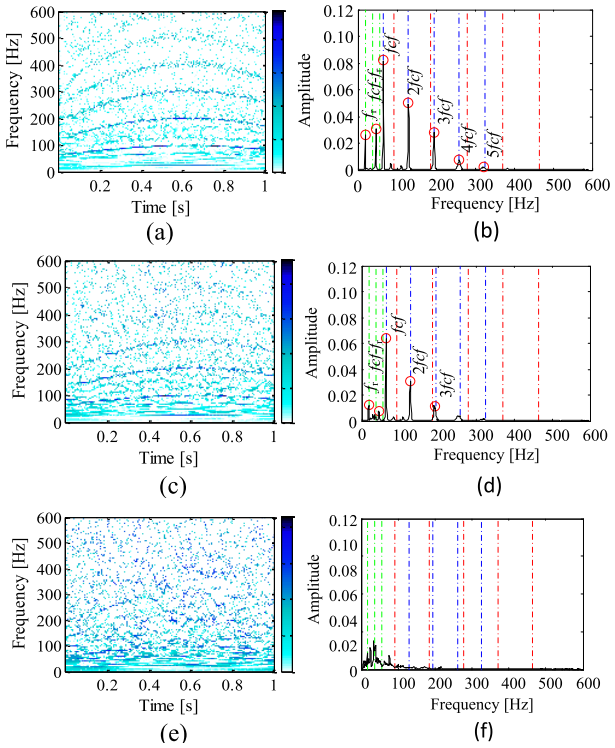

FIGURE 7. Simulated cases under different noise levels: (a), (c) and (e) are TFRs of the simulated signals under SNR of 0, −5 and −10 dB respectively, (b), (d) and (f) are TFRO spectra of (a), (c) and (e) respectively.

To further testify the robustness of the proposed method to noise, more simulated signals under higher noise levels are analyzed. The ConceFT-based TFRs of the envelope signals and the TFRO spectra under SNR of 0 dB, −5 dB, and −10 dB are plotted in Fig. 7. With the rise of noise intensity, it is increasingly difficult to identify the IF from the envelope. For the TFR under SNR of −10 dB, the TF ridges are submerged by the background noise. Correspondingly, no prominent peak is revealed as expected in the TFRO spectrum. Therefore, for the simulated signals under SNR of 10 dB, 0 dB, and −5 dB, the TFRO method performs well in pinpointing the relevant frequency components of bearing signals. If the noise level is too high, the effectiveness of the proposed method is not ideal. It should be noted that, when there are signals with too strong noise, the filtering techniques such as EMD, spectral kurtosis and singular spectrum analysis can be utilized to reduce the noise interference to a certain extent.

V. EXPERIMENTAL EVALUATION

A. EXPERIMENTAL SETTINGS

To further validate the performance of the proposed method, the experimental signal is measured using a vibration test rig at the Beijing Jiaotong University of China. To better describe the assembly relation of different parts, the diagram of experimental setup is plotted in Fig. 8. An accelerometer (CA-YD-1181) is mounted on the top of bearing support to collect the vibration signal. An encoder (KSWL-3806-20) is

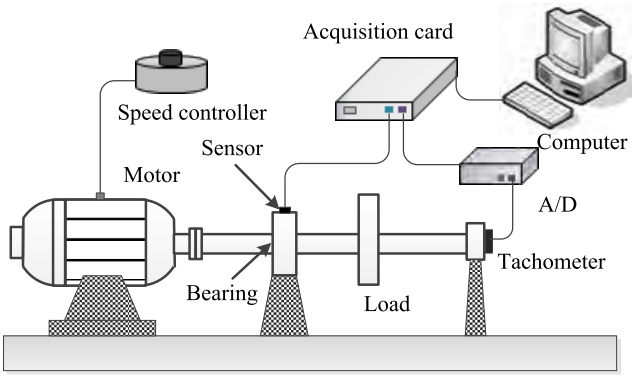

FIGURE 8. Experimental setup.

installed at the end of the shaft to record the speed pulse. The model of acquisition card is DE6231. The rotating speed is adjusted by the speed controller (TDGC2-O.5kVA).

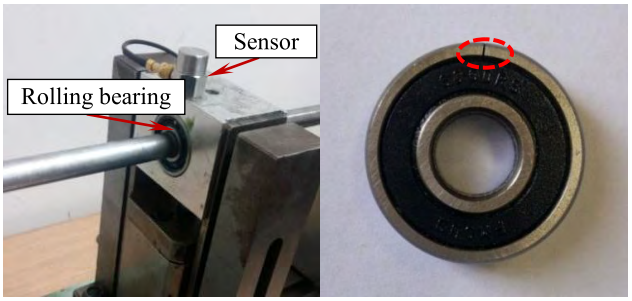

FIGURE 9. Experimental bearing.

To mimic the localized fault, one crack is manufactured in the outer race of the tested rolling bearing. The local graph of bearing installation and bearing are illustrated in Fig. 9. The sampling frequency is set to 24 000 Hz and the data is collected for 2 seconds. The type of the tested bearing is 6000. According to the geometry parameters of the bearing, the fault characteristic coefficients (FCCs) of outer race, inner race, and rolling element are calculated. Fig. 10 shows the geometry of rolling element bearing. The detailed parameters of the bearing are listed in Table 2.

TABLE 2. Parameters of the rolling element bearing.

Parameter	value
Bearing type	6000
Number of rolling element	7
Rolling element diameter	4.8 mm
Pitch diameter	17.65 mm
Contact angle	0 rad
FCC of outer race (C_{outer})	2.55
FCC of inner race (C_{inner})	4.45
FCC of rolling element (C_{ball})	1.7

B. VALIDATION OF PROPOSED METHOD

The time domain waveform of the raw vibration and its corresponding rotating speed are shown in Fig. 11 (a) and (f). The speed trend is calculated by the polynomial fitting

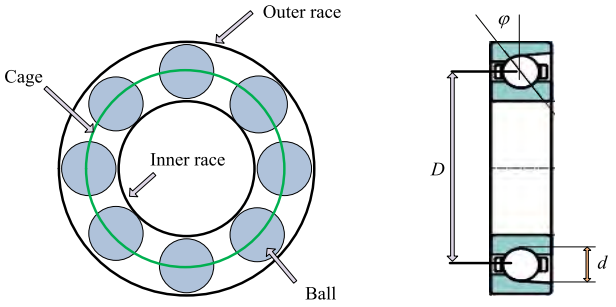

FIGURE 10. The geometry of rolling element bearing.

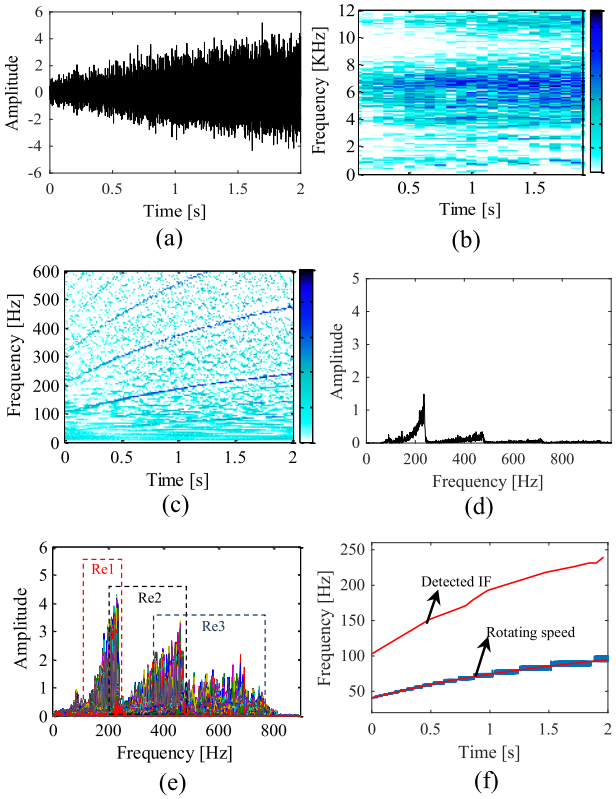

FIGURE 11. Experimental cases: (a) waveform, (b) TFR of the raw signal, (c) TFR of the envelope signal, (d) frequency distribution, (e) frequency spectrum of the envelope, (f) IF extracted by CPP.

based on the pulse interval and the parameters of encoder. Fig. 11 (b) and (c) are the TFRs of the raw signal and the envelope signal respectively. As observed, there is no obvious TF ridge in the TFR of raw signal. In the TFR of the envelope, clear TF ridges are revealed following the rotating speed variation profile. However, the bearing fault cannot be identified by these TF ridges without the reference of measured rotational speed and prior knowledge, not to mention the fault location. As mentioned before, rotor unbalance, even the unavoidable manufacturing errors in some mechanical equipment may produce the same TF trends. The direct projection of the envelope TFR to the frequency axis and the envelope spectrum are plotted in Fig. 11 (d) and (e) respectively. The characteristic frequencies are distributed in wide ranges, resulting in frequency smearing. Fig. 11 (f) shows the IF $f(t)$ detected by CPP, which also follows the speed change profile.

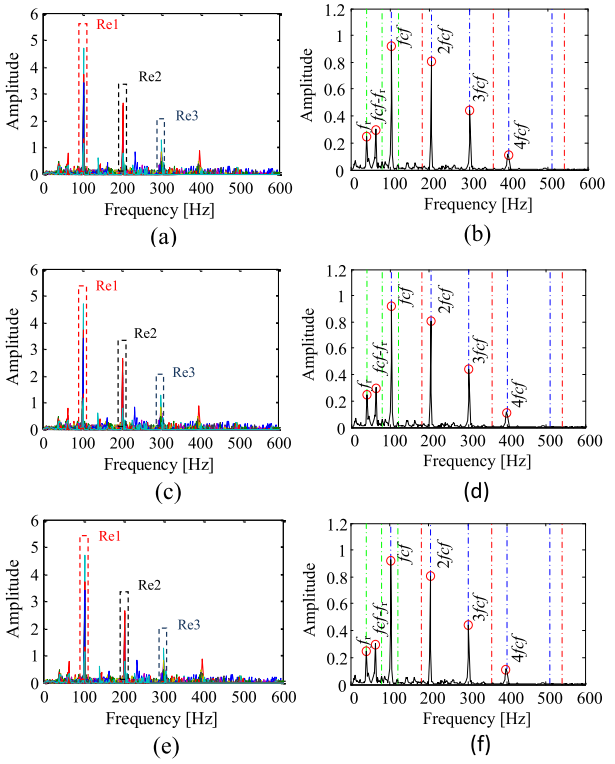

FIGURE 12. TF reconfiguration results guided by different IFs: (a), (c) and (d) are the projections of reconfigured TFRs guided by the detected $f(t)$, $1/2\,f(t)$ and $2\,f(t)$ respectively, (b), (d) and (f) are the corresponding TFRO spectra of (a), (c) and (e) respectively.

Fig. 12 (a) and (b) show the projection of the reconfigured TFR and the TFRO spectrum guided by the detected $f(t)$. By the TF reconfiguration, the distributions of characteristic frequency components are effectively condensed in the projection figure, but the bearing fault pattern still cannot be identified conveniently because the direct projection is sensitive to the noise. Fortunately, the modulation characteristic frequency components are highlighted by the TFRO approach. The existence of bearing fault is usually determined by the identification of FCF and then the fault type is confirmed with the help of modulation rotation speed. In the TFRO spectrum, besides the FCF, the peaks at the locations associated with modulation rotation speed f_r and one sideband $fcf - f_r$ appear. The FCF and its harmonics indicate the existence of bearing fault. To identify the fault type, the ratio of fcf to f_r is calculated $C = fcf/f_r$, which corresponds to the FCC of outer race. The value of sideband further confirms that the outer race fault does exist. The results are consistent with the actual experimental settings.

To test the influence of the reference IF on the result spectrum, the projections of reconfigured TFR guided by $1/2\,f(t)$ and $2f(t)$ are plotted in Fig. 12 (c) and (e) respectively.

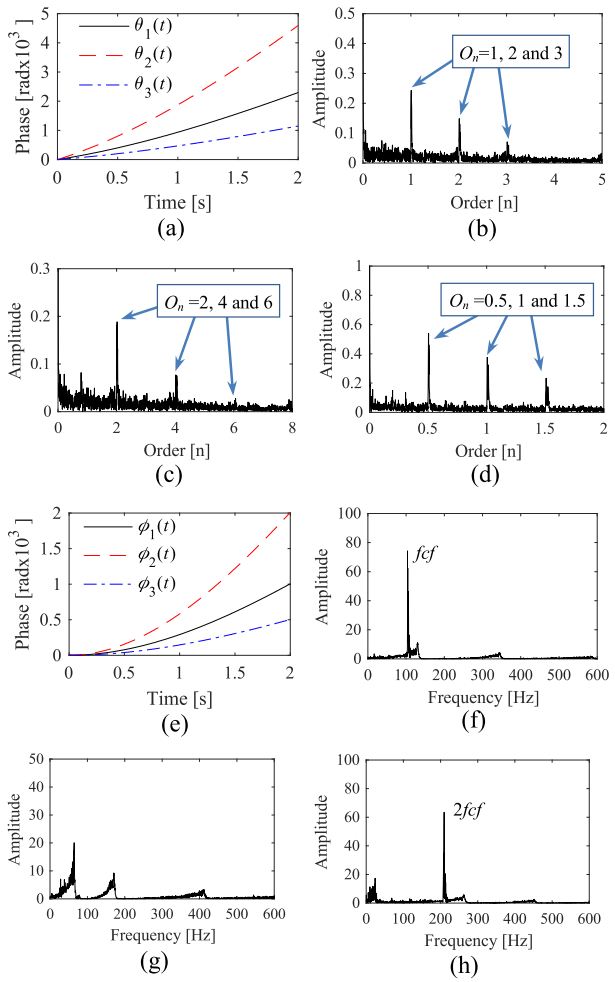

FIGURE 13. Comparison results: (a) phase functions $\theta_1(t)$, $\theta_2(t)$ and $\theta_3(t)$ in the OT applications, (b), (c) and (d) are the order spectrums based on the phase functions $\theta_1(t)$, $\theta_2(t)$ and $\theta_3(t)$ respectively, (e) phase functions $\varphi_1(t)$, $\varphi_2(t)$ and $\varphi_3(t)$ in the GD applications, (f), (g) and (h) are the demodulation spectrums based on $\varphi_1(t)$, $\varphi_2(t)$ and $\varphi_3(t)$ respectively.

Correspondingly, the TFRO spectra guided by $1/2\,f(t)$ and $2f(t)$ are shown in Fig. 12 (d) and (f) respectively. Compared with those spectra, the TFRO results are hardly affected by the reference IFs, i.e., the TF reconfiguration produces a consistent result spectrum guided by different IFs detected from the signal, avoiding the difficulty of identifying which component the extracted IF belongs to.

C. COMPREHENSIVE COMPARISON

To validate the superiority of the method, both OT and GD are utilized to analyze the experimental signal for comparison.

First, the processing results of OT are analyzed. Fig. 13 (a) shows the reference phase functions of the resampling operation, in which $\theta_1(t)$, $\theta_2(t)$ and $\theta_3(t)$ are derived by $\theta_i(t) = 2\pi C_i \int f(t)\mathrm{d}(t)$ (where $i = 1, 2$ and 3, $C_i = 1$, 1/2 and 2). Fig. 13 (b)-(d) display the order spectrums produced by applying OT to the vibration signal guided by $\theta_1(t)$, $\theta_2(t)$ and $\theta_3(t)$ respectively. It can be observed that obvious peaks related to FCF and its harmonics are pinpointed in the three order spectrums. However, the locations of the peaks corresponding to the same frequency component in different spectrums are changed (which is explained in Section II-B) and the order values are not related to the fault location directly. Moreover, as for Fig. 13 (b) and (c), the modulation rotating frequency in the lower frequency region is overwhelmed by noise. Although the modulation frequency and one sideband are revealed in Fig. 13 (d), they are still surrounded with noise and not as clear as the TFRO-based results (Fig. 13 (b), (d) and (f)).

Second, the commonly used GD is performed to validate the merit of the proposed method. Fig. 13 (e) shows the phase functions $\varphi_1(t)$, $\varphi_2(t)$ and $\varphi_3(t)$ corresponding to components $f(t)$, $1/2f(t)$ and $2f(t)$ respectively, which are calculated by $\varphi_i(t) = 2\pi C_i \int [f(t) - f_0]\mathrm{d}(t)$ (where f_0 represents the initial frequency of $f(t)$, $i = 1, 2$ and 3, $C_i = 1$, 1/2 and 2). Fig. 13 (f)-(h) show the demodulation spectrums based on $\varphi_1(t)$, $\varphi_2(t)$ and $\varphi_3(t)$ respectively. From those figures, it can be found that only one component is revealed in Fig. 13 (f) and (h) respectively, i.e., the component *fcf* and its second harmonic *2fcf* are demodulated based on $\varphi_1(t)$ and $\varphi_3(t)$ respectively. As for Fig. 13 (g), no prominent peaks appear which indicates that no components are demodulated via $\varphi_2(t)$ effectively.

As analyzed in Section V-B, guided by different IFs (i.e. $f(t)$, $1/2f(t)$ and $2f(t)$), the TFRO based spectrums don't change with the variation of guidances which simplifies the fault localization. More importantly, the proposed method can produce clear spectrum consisting of the FCF and its harmonics as well as the modulation rotating frequency guided by one arbitrary IF. The comparison results confirm the superiority of the proposed method.

VI. CONCLUSION

A novel ConceFT-based TFRO method is proposed for bearing fault diagnosis under nonstationary conditions. The characteristic frequency is extracted from the envelope signal by CPP and the high resolution TFR of the envelope with sharp TF ridges is obtained by exploiting the merits of the ConceFT. The TFRO spectrum is implemented by reconfiguring the fine TFR according to the proposed algorithm with the extracted IF as a trigger reference. The major contributions of the proposed method include:

(a) It avoids the spectrum smearing caused by the speed fluctuation and therefore pinpoints the time-varying characteristic frequency components in the order spectrum free from the encoder/tachometer;

(b) It produces a consistent spectrum guided by different IFs, i.e., arbitrary IF extracted from the signal can guide the operation, avoiding the difficulty of identifying which frequency component the IF belongs to;

(c) It reveals all frequency components guided by only one detected IF in an order spectrum and hence avoids the difficulty in calculating the phase functions of other frequency components by the detected IF.

In this preliminary study, the proposed method was demonstrated to be effective for rolling bearing fault diagnosis under speed fluctuation condition. Further studies will be carried out to evaluate the effectiveness of the method in extracting the fault features of more complex rotating equipment such as planetary gearboxes.

REFERENCES

[1] L. Cui, J. Huang, and F. Zhang, "Quantitative and localization diagnosis of a defective ball bearing based on vertical–horizontal synchronization signal analysis," *IEEE Trans. Ind. Electron.*, vol. 64, no. 11, pp. 8695–8706, Nov. 2017.

[2] T. Wang, Q. Han, F. Chu, and Z. Feng, "A new SKRgram based demodulation technique for planet bearing fault detection," *J. Sound Vib.*, vol. 385, pp. 330–349, Dec. 2016.

[3] Y. Zhang, W. Lu, and F. Chu, "Planet gear fault localization for wind turbine gearbox using acoustic emission signals," *Renew. Energy*, vol. 109, pp. 449–460, Aug. 2017.

[4] L. Duan, M. Yao, J. Wang, T. Bai, and L. Zhang, "Segmented infrared image analysis for rotating machinery fault diagnosis," *Infr. Phys. Technol.*, vol. 77, pp. 267–276, Jul. 2016.

[5] Z. Peng and N. Kessissoglou, "An integrated approach to fault diagnosis of machinery using wear debris and vibration analysis," *Wear*, vol. 255, nos. 7–12, pp. 1221–1232, 2003.

[6] T. H. Loutas, D. Roulias, E. Pauly, and V. Kostopoulos, "The combined use of vibration, acoustic emission and oil debris on-line monitoring towards a more effective condition monitoring of rotating machinery," *Meth. Syst. Signal Process.*, vol. 25, no. 4, pp. 1339–1352, May 2011.

[7] J. J. Wang, R. X. Gao, and R. Q. Yan, "A hybrid approach to bearing defect diagnosis in rotary machines," *CIRP J. Manuf. Sci. Technol.*, vol. 5, no. 4, pp. 357–365, 2012.

[8] L. Cui, N. Wu, C. Ma, and H. Wang, "Quantitative fault analysis of roller bearings based on a novel matching pursuit method with a new step-impulse dictionary," *Meth. Syst. Signal Process.*, vols. 68–69, pp. 34–43, Feb. 2016.

[9] Z. Li, X. Yan, C. Yuan, Z. Peng, and L. Li, "Virtual prototype and experimental research on gear multi-fault diagnosis using wavelet-autoregressive model and principal component analysis method," *Meth. Syst. Signal Process.*, vol. 25, no. 7, pp. 2589–2607, Oct. 2011.

[10] H. Zhou, J. Chen, G. Dong, and R. Wang, "Detection and diagnosis of bearing faults using shift-invariant dictionary learning and hidden Markov model," *Meth. Syst. Signal Process.*, vols. 72–73, pp. 65–79, May 2016.

[11] Y. Li, Y. Yang, G. Li, M. Xu, and W. Huang, "A fault diagnosis scheme for planetary gearboxes using modified multi-scale symbolic dynamic entropy and mRMR feature selection," *Meth. Syst. Signal Process.*, vol. 91, pp. 295–312, Jul. 2017.

[12] Y. Li, G. Li, Y. Wei, B. Liu, and X. Liang, "Health condition identification of planetary gearboxes based on variational mode decomposition and generalized composite multi-scale symbolic dynamic entropy," *ISA Trans.*, vol. 81, pp. 329–341, Oct. 2018, doi: 10.1016/j.isatra.2018.06.001.

[13] Y. Lei, Z. Liu, X. Wu, N. Li, W. Chen, and J. Lin, "Health condition identification of multi-stage planetary gearboxes using a mRVM-based method," *Mech. Syst. Signal Process.*, vols. 60–61, no. 8, pp. 289–300, Aug. 2015.

[14] T. Y. Wang, F. L. Chu, and Z. P. Feng, "Meshing frequency modulation (MFM) index-based kurtogram for planet bearing fault detection," *J. Sound Vib.*, vol. 432, no. 13, pp. 437–453, Oct. 2018.

[15] Y. Li, X. Liang, M. Xu, and W. Huang, "Early fault feature extraction of rolling bearing based on ICD and tunable Q-factor wavelet transform," *Meth. Syst. Signal Process.*, vol. 86, pp. 204–223, Mar. 2017.

[16] D. Liu, W. Cheng, and W. Wen, "Generalized demodulation with tunable E-Factor for rolling bearing diagnosis under time-varying rotational speed," *J. Sound Vib.*, vol. 430, no. 15, pp. 59–74, Sep. 2018.

[17] Y. Lei, J. Lin, Z. He, and M. J. Zuo, "A review on empirical mode decomposition in fault diagnosis of rotating machinery," *Mech. Syst. Signal Process.*, vol. 35, nos. 1–2, pp. 108–126, Feb. 2013.

[18] M. Zhang, T. Wang, T. Tang, M. Benbouzid, and D. Diallo, "An imbalance fault detection method based on data normalization and EMD for marine current turbines," *ISA Trans.*, vol. 68, pp. 302–312, May 2017.

[19] D. He, X. Wang, S. Li, J. Lin, and M. Zhao, "Identification of multiple faults in rotating machinery based on minimum entropy deconvolution combined with spectral kurtosis," *Mech. Syst. Signal Process.*, vol. 81, no. 15, pp. 235–249, Dec. 2016.

[20] T. Wang, F. Chu, Q. Han, and Y. Kong, "Compound faults detection in gearbox via meshing resonance and spectral kurtosis methods," *J. Sound Vib.*, vol. 392, pp. 367–381, Mar. 2017.

[21] C. Yi, Y. Lv, Z. Dang, H. Xiao, and X. Yu, "Quaternion singular spectrum analysis using convex optimization and its application to fault diagnosis of rolling bearing," *Measurement*, vol. 103, pp. 321–332, Jun. 2017.

[22] K. R. Fyfe and E. D. S. Munck, "Analysis of computed order tracking," *Mech. Syst. Signal Process.*, vol. 11, pp. 187–205, Mar. 1997.

[23] J. Cheng, K. Zhang, and Y. Yang, "An order tracking technique for the gear fault diagnosis using local mean decomposition method," *Mech. Mach. Theory*, vol. 55, pp. 67–76, Sep. 2012.

[24] Y. Li, K. Ding, G. He, and X. Jiao, "Non-stationary vibration feature extraction method based on sparse decomposition and order tracking for gearbox fault diagnosis," *Measurement*, vol. 124, pp. 453–469, Aug. 2018.

[25] T. Yang, Y. Guo, X. Wu, J. Na, and R.-F. Fung, "Fault feature extraction based on combination of envelope order tracking and cICA for rolling element bearings," *Meth. Syst. Signal Process.*, vol. 113, pp. 131–144, Dec. 2018.

[26] W. Cheng, R. X. Gao, J. Wang, T. Wang, W. Wen, and J. Li, "Envelope deformation in computed order tracking and error in order analysis," *Mech. Syst. Signal Process.*, vol. 48, nos. 1–2, pp. 92–102, Oct. 2014.

[27] Y. Wang, G. Xu, A. L. Luo, L. Liang, and K. Jiang, "An online tacholess order tracking technique based on generalized demodulation for rolling bearing fault detection," *J. Sound Vib.*, vol. 367, pp. 233–249, Apr. 2016.

[28] T. Wang, M. Liang, J. Li, W. Cheng, and C. Li, "Bearing fault diagnosis under unknown variable speed via gear noise cancellation and rotational order sideband identification," *Mech. Syst. Signal Process.*, vols. 62–63, pp. 30–53, Oct. 2015.

[29] D. Zhao, J. Li, and W. Cheng, "Feature Extraction of faulty rolling element bearing under variable rotational speed and gear interferences conditions," *Shock Vib.*, vol. 2015, Nov. 2015, Art. no. 425989.

[30] G. He, K. Ding, W. Li, and X. Jiao, "A novel order tracking method for wind turbine planetary gearbox vibration analysis based on discrete spectrum correction technique," *Renew. Energy*, vol. 87, pp. 364–375, Mar. 2016.

[31] M. Zhao, J. Lin, X. Xu, and Y. Lei, "Tacholess envelope order analysis and its application to fault detection of rolling element bearings with varying speeds," *Sensors*, vol. 13, pp. 10856–10875, Aug. 2013.

[32] T. Wang, M. Liang, J. Li, and W. Cheng, "Rolling element bearing fault diagnosis via fault characteristic order (FCO) analysis," *Mech. Syst. Signal Process.*, vol. 45, pp. 139–153, Mar. 2014.

[33] S. Olhede and A. T. Walden, "A generalized demodulation approach to time-frequency projections for multicomponent signals," *Proc. R. Soc. Lond. A, Math. Phys. Eng. Sci*, vol. 461, no. 2059, pp. 2159–2179, 2005.

[34] C. Li and M. Liang, "A generalized synchrosqueezing transform for enhancing signal time–frequency representation," *Signal Process.*, vol. 92, no. 9, pp. 2264–2274, Sep. 2012.

[35] Z. Feng, X. Chen, M. Liang, and F. Ma, "Time–frequency demodulation analysis based on iterative generalized demodulation for fault diagnosis of planetary gearbox under nonstationary conditions," *Mech. Syst. Signal Process.*, vols. 62–63, pp. 54–74, Oct. 2015.

[36] D. Zhao, J. Li, and W. Cheng, "Compound faults detection of rolling element bearing based on the generalized demodulation algorithm under time-varying rotational speed," *J. Sound Vib.*, vol. 378, pp. 109–123, Sep. 2016.

[37] Z. Feng, X. Chen, and M. Liang, "Joint envelope and frequency order spectrum analysis based on iterative generalized demodulation for planetary gearbox fault diagnosis under nonstationary conditions," *Mech. Syst. Signal Process.*, vols. 76–77, pp. 242–264, Aug. 2016.

[38] E. J. Candes, P. R. Charlton, and H. Helgason, "Detecting highly oscillatory signals by chirplet path pursuit," *Appl. Comput. Harmon. Anal.*, vol. 24, no. 1, pp. 14–40, 2008.

[39] I. Daubechies, Y. Wang, and H.-T. Wu, "ConceFT: Concentration of frequency and time via a multitapered synchrosqueezed transform," *Philos. Trans. Roy. Soc. London A, Math. Phys. Sci.*, vol. 374, no. 2065, p. 20150193, Apr. 2015.

[40] Z. Feng, X. Chen, and T. Wang, "Time-varying demodulation analysis for rolling bearing fault diagnosis under variable speed conditions," *J. Sound Vib.*, vol. 400, pp. 71–85, Jul. 2017.

[41] Z. Feng, M. Liang, and F. Chu, "Recent advances in time–frequency analysis methods for machinery fault diagnosis: A review with application examples," *Mech. Syst. Signal Process.*, vol. 38, no. 1, pp. 165–205, Jul. 2013.
[42] F. Hlawatsch and G. F. Boudreaux-Bartels, "Linear and quadratic time-frequency signal representations," *IEEE Signal Process. Mag.*, vol. 9, no. 2, pp. 21–67, Apr. 1992.
[43] R. Yan, R. X. Gao, and X. Chen, "Wavelets for fault diagnosis of rotary machines: A review with applications," *Signal Process.*, vol. 96, no. 5, pp. 1–15, Mar. 2014.
[44] L. Cohen, "Time-frequency distributions—A review," *Proc. IEEE*, vol. 77, no. 7, pp. 941–981, Jul. 1989.
[45] A. H. Nuttall and E. Bedrosian, "On the quadrature approximation to the Hilbert transform of modulated signals," *Proc. IEEE*, vol. 54, no. 10, pp. 1458–1459, Oct. 1966.
[46] I. Daubechies, J. Lu, and H. T. Wu, "Synchrosqueezed wavelet transforms: An empirical mode decomposition-like tool," *Appl. Comput. Harmon. Anal.*, vol. 30, no. 2, pp. 243–261, Mar. 2011.

DONGDONG LIU received the master's degree in mechanical manufacturing and automation from Beijing Jiaotong University, China, in 2017, where he is currently pursuing the Ph.D. degree in mechanical engineering with the School of Mechanical Electronic and Control Engineering. His research interests include machinery fault diagnosis and signal processing.

WEIDONG CHENG received the Ph.D. degree from the Department of Precision Instruments, Tsinghua University, China, in 2001. He is currently a Processor with the School of Mechanical Electronic and Control Engineering, Beijing Jiaotong University, China. His research interests include intelligent measurement and control of manufacturing equipment, pattern recognition, and signal processing.

WEIGANG WEN received the Ph.D. degree in traffic information engineering and control from Beijing Jiaotong University, China, in 2006. He is currently an Associate Professor with the School of Mechanical Electronic and Control Engineering, Beijing Jiaotong University. His research interests include intelligent measurement and control of manufacturing equipment and fault diagnosis.